Int. J. Solids Structures, 1970, Vol. 6, pp. 1157 to 1172. Pergamon Press. Printed in Great Britain

LONGITUDINAL WAVE PROPAGATION TESTS AND THE EXPERIMENTAL DETERMINATION OF THE DYNAMIC STRESS–STRAIN CHARACTERISTICS OF PURE IRON†

HAL WATSON, JR.

Southern Methodist University, Institute of Technology, Dallas, Texas

Abstract—Short cylindrical specimens of Armco iron were tested at room temperature under compressive, axial loads at strains up to 0·6% and strain rates up to 10^3 in./in. sec. During loading, the axial stress was measured with a thin piezoelectric disk inserted between the specimen and the loading bar. The surface strain was measured with conventional epoxy-backed, foil strain gages, and the strain rate deduced by differentiating the strain–time data record. The stress, strain and strain rate data were plotted and were found to be approximated by a particular constitutive functional. The constitutive equation was then used along with the governing equations of motion and continuity in finding a numerical solution to the problem of a one-dimensional plastic wave propagating in a rate sensitive bar caused by an initial axial stress $\sigma(0, t)$. The numerical solutions for both stress and strain were found to agree favorably with the stress and strains which were measured, with embedded piezoelectric disks and strain gages, respectively, at two locations along a long iron bar wave propagation test. Thus, a constitutive relationship found to approximate the stress–strain–strain rate data generated in a short specimen impact test can be used to predict, with reasonably good agreement, the stresses and the strains measured in a long bar propagation test. This agreement indicates that the approximate constitutive function is a valid description of the flow properties of the material for the ranges of strain and strain rate observed.

INTRODUCTION

IT IS generally accepted that most engineering materials are, to some degree, rate sensitive; that is, the materials exhibit the property in a dynamic test, of being able to support a greater stress, at a particular value of strain, than that observed, at the same strain, in a quasi-static test. It has been observed that some materials, such as the body-centered-cubic metals, are highly rate sensitive at low rates of straining, while other materials, such as the face-centered-cubic metals, are only slightly rate sensitive under the extremes of impact loading rates [1–5]. These observations can be explained qualitatively by the dislocation theory of plastic deformation, which attributes the strain rate effect to the obstruction of the progress of dislocations as they migrate through the material. Body-centered-cubic metals have been found to contain more dislocation locking mechanisms and to possess fewer slip modes, and therefore to offer more obstruction to dislocations, than the face-centered-cubics. It has been shown that macroscopic creep, quasi-static stress–strain, and impact tests can all be interpreted in terms of a general strain rate relationship that is based on a microdynamical theory of dislocations [6].

In order to determine the exact degree of rate sensitivity of a material the states of stress and strain must be measured simultaneously at a single material point over a wide range of constant strain rates. Even if such ideal measurements could be performed, it would be necessary to assume that the measurements at that single point are representative of

†This research was sponsored in part by the Army Research Office Contract DA-31-124-ARO-D-229, the National Science Foundation Grant No. GK-3493, and by the Office of Naval Research Contract No. N00014-68-A-0515.

measurements made at every other point in the entire batch of material; that is, that the material is perfectly homogeneous in its properties. To compound the difficulties, any constitutive relationship inferred from the measurements is valid only for the particular environmental conditions of the tests. Changes in temperature and pressure can greatly affect the stress–strain–strain rate relationship [1, 2, 4, 7].

Several techniques of determining the dynamic stress–strain characteristics of metals have been employed [1–5, 7, 8]. Each save three [3, 4, 7] has employed a technique of measurement that does not permit independent measurements of both stress and strain. Each has measured only strain, particle velocity, or stress at one or more locations. Furthermore, each has assumed a one-dimensional state of stress or strain in interpreting the properties of the material from the experimental data. Often, as in the references cited above, conflicting interpretations of the test data for the same material can be found. Karnes and Ripperger [3] have found from data obtained from longitudinal impact experiments on short specimens that pure annealed aluminum is significantly strain rate sensitive, while Bell [5] has interpreted data from a wave propagation test on a long bar of the same material that the material is strain rate insensitive. Hauser *et al.* [8] also found from compressional impact tests using a split-Hopkinson pressure bar that pure aluminum is rate sensitive.

Several reasons can be offered to explain why the above-mentioned investigators have reached different conclusions with regard to the dynamic stress–strain characteristics of aluminum. First, in interpreting the data, each has assumed that a one-dimensional theory governs in the large stress rate and strain rate regions in which he gathered the data. In such regions, the assumption of a one-dimensional theory is highly questionable. Devault [9] has shown that the two-dimensional effect of lateral inertia becomes important in regions of high stress rate. Second, stress and strain data are not measured independently in the specimen itself, as in the case of the split-Hopkinson pressure bar method in which only strain measurements are made on the elastic pressure bars near the specimens. This leads to averaging the stress, strain and strain rate over the entire length of the specimen when reducing the data. Third, in the wave propagation experiments in which only strain is measured, the average wave speed of a given level of plastic strain is deduced from the strain-time data at several locations along the bar and used to calculate the stress, assuming the material to be strain rate independent. Analysis of the data obtained in the latter type of experiment presupposes that the strain wave front profile is a unique property of the constitutive equation. However, Ripperger and Watson [10] have shown from their theoretical calculations, using both rate independent and rate dependent constitutive equations in the one-dimensional theory, that very nearly the same wave front profile can be obtained for materials only mildly strain rate sensitive, at low strain rates and stress rates where a one-dimensional theory is valid.

It is implied in the above paragraphs that stress, strain and strain rate must be measured in the specimen itself in order to obtain data that will allow the determination of the constitutive equation of the material. Furthermore, one must take into consideration any departures from whatever theory is used in interpreting the data. Assuming lateral inertia effects to be negligible in regions of high stress rates and strain rates which are necessary to test slightly rate sensitive materials for strain rate sensitivity can lead to serious errors in data interpretation.

The above-mentioned problems are not so difficult whenever highly rate sensitive materials such as Armco iron are tested, for the rate sensitivity is obvious even at very

low strain and stress rates. However, in determining the stress–strain characteristics at the higher rates, the problems concerning lateral inertia become great regardless of the degree of rate sensitivity of the material. In addition, this author has found that whenever a material is assumed to be highly strain rate sensitive, the calculated, theoretical wave front profiles are greatly affected by the functional form and degree of rate sensitivity of the constitutive equation and by the initial conditions used in the calculations [11]. Therefore, meaningful comparisons of both stress and strain data taken from wave propagation experiments can be made with the stresses and strains calculated using a one-dimensional theory and the experimentally determined constitutive equation and the measured initial stress condition, provided the stress and strain rates are not large.

It is the purpose of this paper to show that either short specimen impact tests or long bar propagation tests can be employed to obtain the dynamic stress–strain characteristics of a highly rate sensitive material, such as Armco iron, provided both the stress and the strain are measured directly in the specimen at low stress and strain rates. Furthermore, it is the purpose of this paper to show that the experimentally determined constitutive equation can be used to predict the stresses and strains propagated along a long bar of the material by obtaining a numerical solution to the problem of a one-dimensional wave propagating in a visco-plastic bar as proposed by Malvern [12].

The experimental technique employed in this investigation had been used previously to measure the dynamic stress–strain characteristics of short cylinders of aluminum at normal environmental conditions by Karnes and Ripperger [3], of copper at pressures up to 100 Ksi by Chalupnik and Ripperger [4], and of copper at temperatures up to 1000°F by Watson and Ripperger [7]. This method allows the measurement of all three important quantities—stress, strain and strain rate at essentially the same material location. This author extended the technique used to test the short specimens to measure stress and strain in a long bar propagation test by embedding a piezoelectric disk in the long bar. This is similar to the technique reported by Shea [13] who used an embedded disk to obtain dynamic stress–strain data for lead. However, Shea did not measure the stress at the impact end or the longitudinal strains as this author did. Shea was able to predict the stress at one location and the circumferential strains at several locations using a one-dimensional stress theory that incorporated lateral inertia and strain rate dependence.

EXPERIMENTAL METHOD

The experimental method used in the dynamic testing of the short specimens is a variation of the split-Hopkinson pressure bar technique. However, this variation of the technique does not require the critical assumption of uniformity of stress, strain and strain rate over the entire length of the specimen, an assumption which is necessary in reducing the raw data taken from a split-Hopkinson bar experiment.

This variation of the split-Hopkinson bar technique includes the use of a thin, calibrated, piezoelectric (X-cut quartz) crystal, which is sandwiched between a hardened steel loading bar and the softer specimen, in measuring the average stress over the cross section of the specimen (Fig. 1). On the surface of the specimen, very near the quartz crystal, is mounted an electrical resistance strain gage for measuring the axial strain. The slope of the strain vs. time record is the strain rate. It is assumed that the stress, strain and strain rate are measured at essentially the same material point. It is further assumed in the data reduction

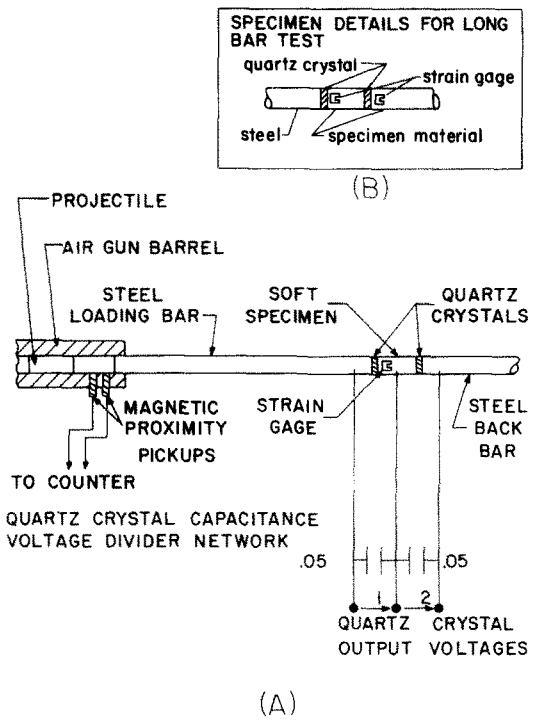

FIG. 1. (A) Schematic of the apparatus for short specimen impact test. (B) Schematic of the alterations in the set-up (A) required for a long bar propagation test.

that: (1) the stress is uniform and axial over the cross section, (2) the difference between the stress at the crystal and the stress on the cross section beneath the strain gage is insignificant, (3) the surface strain is representative of the axial strain at every point on the cross section beneath the gage, and (4) lateral inertia effects on the axial stress are negligible. Arguments in support of each of these assumptions have been made elsewhere [3, 4, 11] but will be outlined in the following paragraphs.

To initiate a typical dynamic test on a short, metal specimen, a flat-nosed hardened steel projectile is propelled along the evacuated barrel of an air gun and is allowed to impact the hardened steel loading bar, one end of which is positioned inside the gun barrel near the muzzle. The impact gives rise to an elastic stress wave, which propagates along the loading bar, through the quartz crystal, and into the specimen. As the stress pulse passes through the quartz crystal into the specimen, a stress exceeding the static yield stress of the material is impressed on the front face of the test specimen, forcing it to be strained into the plastic range. During the plastic deformation, the value of the average stress over the cross section of the specimen is measured by means of the quartz disk which generates an electrical charge proportional to the average stress over the cross section. The charge is then collected on a capacitor and the voltage across the capacitor is measured. It can be shown that the effect on the stress wave due to the presence of the quartz disk is negligible, if the thickness of the disk is small compared to the wavelength of the stress pulse. For a 0·020 in. disk such as that used in these tests the calculated effect is to increase the rise time of the stress pulse by only a microsecond.

The quartz crystal-capacitor system is calibrated for stress by replacing the specimen with a hardened steel load cell calibrated in a static test, and by allowing an elastic wave to propagate through the load cell. The strain measured on the surface of the load cell together with its stress–strain curve is then used to calibrate the quartz disk. A calibration test record is shown in Fig. 2. The system calibration was found to be 26,500 psi/V.

Very near the quartz crystal ($\frac{1}{8}$ in. for 0·50 in. dia. specimen) a foil, resistance strain gage is attached in order to measure the axial surface strain near the disk. The measured value of surface strain at this location is assumed to be representative of the average axial strain over the material cross section beneath the strain gage. This assumption is reasonable from material continuity considerations if after the test, the faces of the extreme ends of the specimen are found to be parallel and no local barreling is evident along the length of the specimen. Although the strain gage and the load transducer are not at the exact same location along the length of the specimen, it can be shown that only in regions of very large time derivatives of stress and of very large strains, is the spatial derivative of stress $\partial\sigma/\partial x$ large. In such regions, the small difference in spatial location does give rise to appreciable error. For dynamic testing of this type in which the stress wave has traveled along a long loading bar and has undergone the subsequent dispersion of its high frequency components, it can be shown that the stress rates are not of sufficient magnitude to cause large spatial errors except very near the wave front. Since stress vs. time is measured, it is a simple matter to limit the selection of stress–strain data to regions of small stress rate.

Errors due to antisymmetric loading were minimized by careful alignment of the loading bar projectile and loading bar specimen interfaces and by use of machine-lapped interfaces. A number of dynamic tests were performed to check the accuracy of alignment

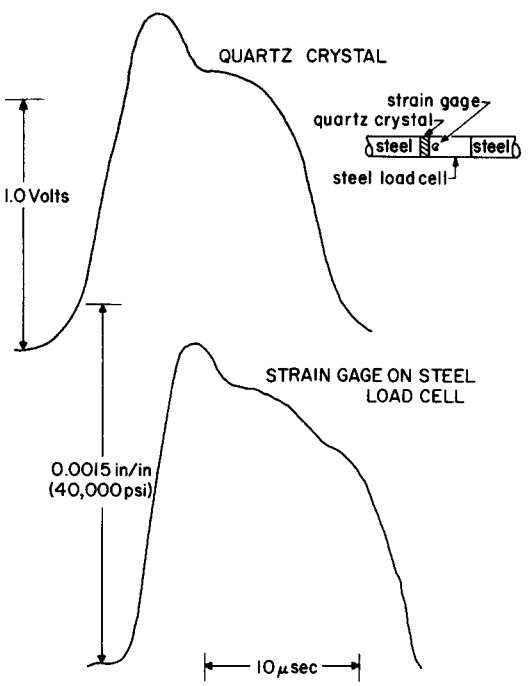

FIG. 2. Quartz crystal calibration record.

and symmetry of loading by separately measuring the strain on diametrically opposed positions at a particular material cross section. For well aligned bars, the strain records are nearly identical. The stress–time record also provides a check on the alignment during each test. This author has found that an incorrect alignment causes the stress–time record to have a greatly increased rise time. A rise time of 5 μsec or less usually accompanies identical strain–time records of the opposing strain gages.

Radial inertia effects

The question always arises in tests of this type as to whether or not the assumptions of one-dimensional stress and of negligible radial inertia effects on the axial stress are valid. In view of the type of loading and the geometry (the wavelength of the axial stress pulse is greater than the diameter of the specimen), the first assumption is reasonable from a theoretical view; however, radial inertia effects on the axial stress are predicted to be significant beyond a certain loading rate. Devault [9] has shown that it is inherently difficult to separate strain rate effects from radial inertia effects in regions of high stress rate. Hunter and Davies [14] have also shown that significant radial inertia effects are to be expected in regions where the time derivative of strain rate is large. This author has observed from the stress and strain records of the tests reported here that the regions of large time derivatives of strain rate occur at times of large stress rate. In tests of this type, it is in these regions of large stress rate in which one must reject the data in order that $\partial\sigma/\partial x$ be negligible (page 1161). Therefore, this author assumes radial inertial effects to be negligible in the regions where the raw data points were selected, regions in which $\partial\sigma/\partial x \simeq 0$.

Specimen preparation

The specimen materials were furnished by the manufacturer in $\frac{3}{4}$ in. rounds, which were turned down to $\frac{1}{2}$ in. rounds in a lathe. The rounds were then cut off to 1 in. lengths and faced off in a lathe. The 1 in. lengths were then annealed in an evacuated furnace for 1 hr at 1500°F and allowed to furnace cool. Each specimen was then lapped flat on each end and prepared for the attachment of the strain gages. Two $\frac{1}{8}$ in. epoxy-backed strain gages were attached, diametrically opposed, onto each specimen $\frac{1}{16}$ in. from one end.

A chemical analysis of random samples of the specimen material, Armco iron, was obtained and revealed the following impurities: 0·02% carbon, 0·012% sulfur and 0·008% phosphorus. Metallograph measurements revealed that there were an average number of 600 grains/mm^2 for a typical annealed specimen.

Test procedure and data selection

The outputs of the stress and strain circuits were connected to a dual-beam, 10 MHz oscilloscope and the oscillograms recorded on Polaroid film. The oscilloscope was triggered by the output voltage of a small piezoelectric accelerometer attached to the surface of the loading bar which responded to the passage of the stress wave. In this way the oscilloscope was synchronized to the event of the stress wave entering the quartz crystal. A typical stress and strain vs. time record taken from the Polaroid photograph and enlarged is shown in Fig. 3. One observes from the figure that during the passage of the wave front the stress rate and rate of change of strain rate are quite large ($\dot{\sigma} \simeq 10^{10}$ psi/sec, $\ddot{\varepsilon} \simeq 3 \times 10^7$ in./in.-sec^2); however, about 10^{-5} sec *after* the passage of the wave front both $\dot{\sigma}$ and $\ddot{\varepsilon}$ are very

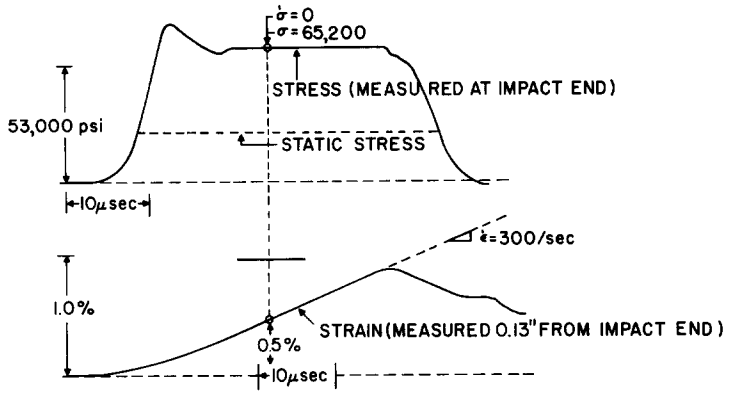

FIG. 3. Typical records of stress and strain vs. time taken from a dynamic test of a shirt specimen.

nearly zero. It is in this region that radial inertia effects and stress gradients are small and where the data for this investigation were selected. The values for the two data points in Fig. 4 are: $\dot{\sigma} \simeq \ddot{\varepsilon} \simeq 0$, $\sigma = 65{,}200$ psi, $\varepsilon = 0{\cdot}5$ per cent and $\dot{\varepsilon} = \dot{\varepsilon}_p = 300$ in./in.-sec.

The data from the short specimen tests are plotted in Fig. 4 in which stress is plotted vs. strain for several strain rates. Also shown on the figure is the quasi-static curve taken from a test in which a hydraulic loading machine was used. The data points for the σ vs. ε at

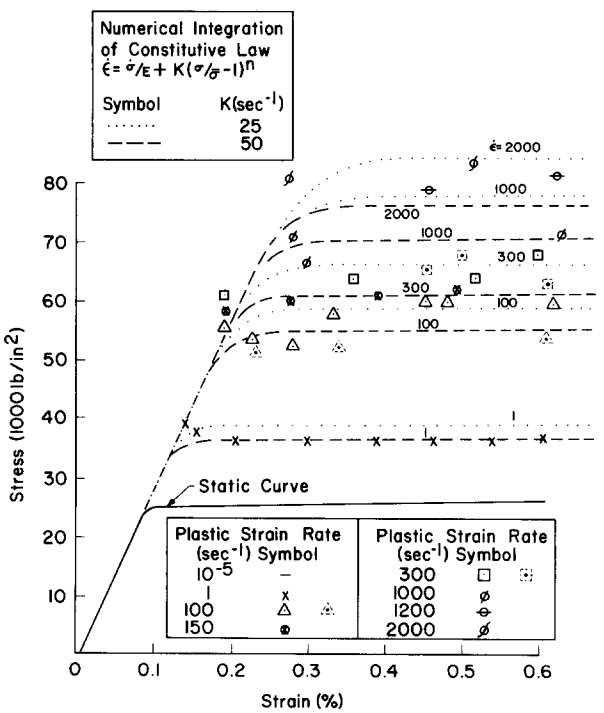

FIG. 4. Stress–strain data at several strain rates for Armco iron at room temperature. Dashed and dotted lines are computed stress–strain curves for the particular constitutive equation shown. Dashed symbols are long bar test data.

$\dot{\varepsilon} = 1$ in./in.-sec were obtained similarly. Since the tests were destructive and the strain rate varied in each test, several specimens had to be tested at each impact velocity. Altogether, ten tests were performed on short cylinders of Armco iron at strain rates up to 10^3 in./in.-sec.

Long bar tests

In a long bar test, the hardened steel back bar used in the short specimen tests is replaced by a long bar of specimen material to which a quartz disk and strain gages are attached. Thus, the short specimen and the back bar of specimen material form a long bar of specimen material with an embedded quartz disk [Fig. 1(b)]. During an impact test each quartz crystal and adjacent set of gages yield the stress and strain-time data at essentially the same location. This author found the effect of the embedded quartz disk on the stress wave to be negligible provided the specimen and back bar were properly aligned and the interfaces properly lapped so that no gaps existed to cause unloading reflections.

The results of a typical long bar test on iron are shown in Fig. 5 for the two strain–time records of the strain gage stations positioned at 0·125 in. and 1·125 in. from the loaded end, and in Fig. 6 for the two stress–time records of the outputs of the quartz disks, positioned at 0·0 in. and 1·0 in. from the loaded end. Each strain record shows a region of high strain rate at the wave front followed by a region of lower strain rate. The level of strain at the wave front is 0·2 per cent or twice the static yield strain. These records verify the prediction of a small amount of plastic strain propagating at the elastic wave speed by the rate dependent theory of Malvern [12]. The high frequency Pochhammer–Chree oscillations are evident in the first stress record. The stress records show a region of very short rise time and high stress rate at the wave front followed by a region of much lower stress rates. A quantitative comparison of the long bar stress, strain and strain rate data is consistent with the data taken from the short specimen tests as demonstrated in Fig. 4 in which the long bar data of this test are plotted along with the short specimen data.

THEORY

The equations used in the mathematical description of a one-dimensional stress wave propagating in a rate sensitive material are those which were introduced by Malvern [12]. One dimensional theory was applicable because of the magnitudes of strains, strain rates and stress rates which were present in the tests. Higher rates would require the use of a two- or three-dimensional theory with all of the complications of programming the equations not to mention those of determining which constitutive relations, what boundary conditions, and what yield conditions to assume [15–17]. Incorrect use of assumptions of these quantities are likely to cause greater errors in solution than a simpler theory.

The governing equations of motion and of continuity are:

$$\frac{\partial \sigma}{\partial x} = \rho \frac{\partial v}{\partial t} \tag{1}$$

$$\frac{\partial v}{\partial x} = \frac{\partial \varepsilon}{\partial t} \tag{2}$$

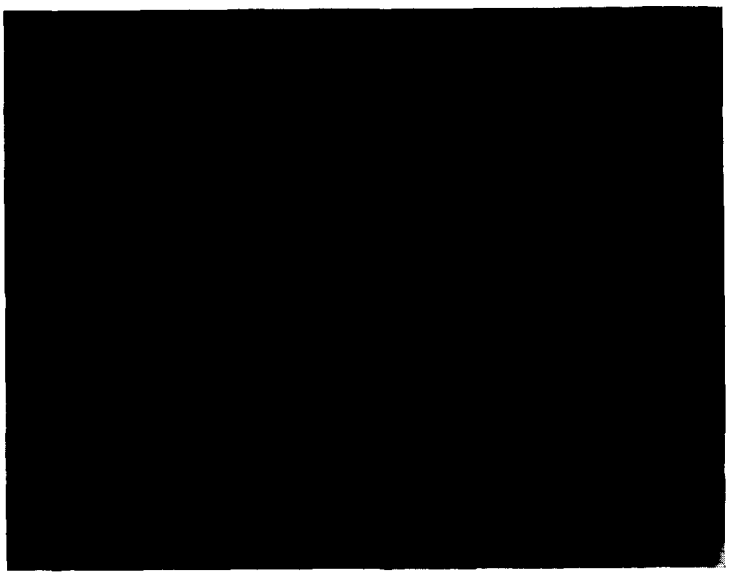

FIG. 5. Typical records of strain vs. time at two locations along a long bar during a propagation test. Distance between calibration dots represents 1·73 per cent strain. Lower trace is for gage at 0·125 in. from impact end. Upper trace is for gage at 1·125 in. from impact end. Horizontal scale is 10 μ sec per main division.

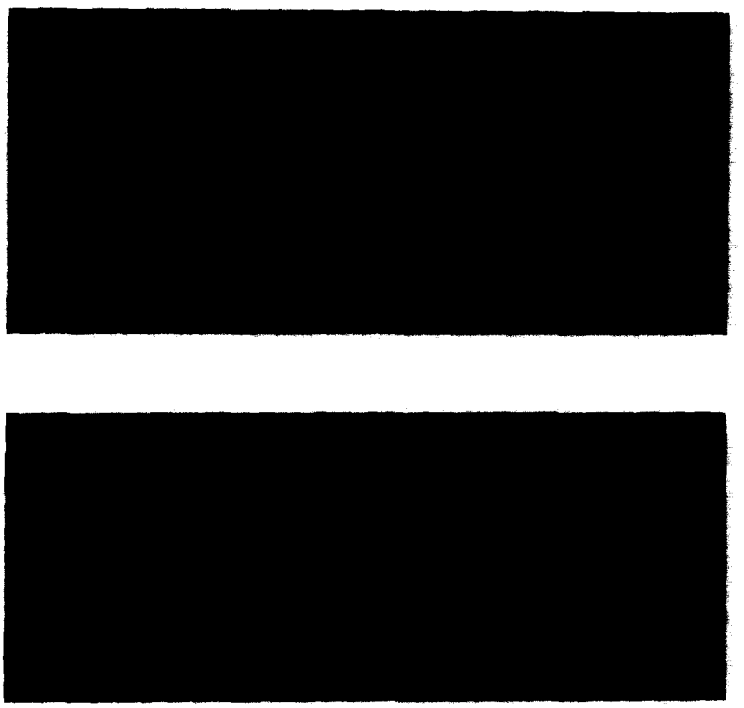

FIG. 6. Typical records of stress vs. time at two locations along a long bar during a propagation test. Distance between calibration dots is 53,000 psi (top) and 47,400 (bottom). Horizontal scale is 10 μ sec per main division. Upper trace is for crystal 0·0 in. from impact end. Lower trace is for crystal at 1·0 in. from impact end.

where x is the Lagrangian coordinate of a material point originally a distance x from the loaded end, σ is the axial stress, ρ is the original mass density, v is the particle velocity and ε is the strain. The strain is assumed to be comprised of two parts—the elastic part ε_E and the plastic part ε_p—such that

$$\varepsilon = \varepsilon_E + \varepsilon_p;$$

therefore,

$$\frac{\partial \varepsilon}{\partial t} = \frac{\partial \varepsilon_E}{\partial t} + \frac{\partial \varepsilon_p}{\partial t}. \tag{3}$$

It is assumed that

$$\frac{\partial \varepsilon_E}{\partial t} = \frac{1}{E}\frac{\partial \sigma}{\partial t} \tag{4}$$

in which E is Young's modulus and

$$\frac{\partial \varepsilon_p}{\partial t} = g(\sigma, \varepsilon). \tag{5}$$

The latter is the so-called "g" function which must be determined from experimental data. Equations (3)–(5) can be combined to form

$$\frac{\partial \varepsilon}{\partial t} = \frac{1}{E}\frac{\partial \sigma}{\partial t} + g(\sigma, \varepsilon), \tag{6}$$

which is the constitutive equation. Equations (1), (2) and (6) form a hyperbolic set of first order partial differential equations which can be solved by means of the method of characteristics [11, 12]. After applying the method of characteristics, a new set of characteristic differential equations emerge which are valid along certain characteristic directions. These are:

Characteristic equation	Differential equation for characteristic curves
$d\sigma - \rho C_0\, dv = -g(\sigma, \varepsilon)\, dt$	$dx = C_0\, dt$
$d\sigma + \rho C_0\, dv = -g(\sigma, \varepsilon)\, dt$	$dx = -C_0\, dt$
$d\sigma - E\, d\varepsilon = -g(\sigma, \varepsilon)\, dt$	$dx = 0$

(7)

where $C_0 = (E/\rho)^{\frac{1}{2}}$. The characteristic equations are usually nonlinear because of the nonlinear character of $g(\sigma, \varepsilon)$. Although few closed form solutions are attainable for these equations, they are easily programmed for a digital computer after the usual finite difference approximations for the derivatives have been made. The ease of programming is due to the fact that the characteristic curves are straight lines in the x–t plane (Fig. 7). The only difficulties which arise are due to the fact that finite differencing the characteristic equations yields a set of three nonlinear algebraic equations to be solved at each point (x, t) in the characteristic plane for σ, ε and v. The problem is thus reduced to solving for the roots of a set of three nonlinear, algebraic equations at each point in the characteristic plane. In the program, a scheme employing a predictor-corrector, iterative procedure is followed at each point until a predicted set of values of σ, ε, v agree with a previously predicted set

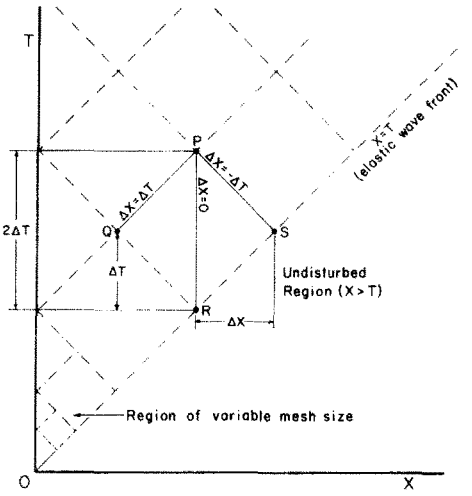

FIG. 7. Characteristic plane—after non-dimensionalizing all variables the characteristic lines $x = 0$, $x = C_0 t$ and $x = -C_0 t$ becomes $X = 0$, $X = T$ and $X = -T$. X and T are non-dimensional variables.

to a certain preset number of digits. There is no problem of computation along the line $x = 0$ since the stress is defined on that boundary. However, along the line $x = C_0 t$ the following jump conditions must be employed.

$$\begin{aligned} \Delta\sigma &= -\rho C_0 \Delta v \\ \Delta v &= -C_0 \Delta\varepsilon \end{aligned} \tag{8}$$

where Δ denotes a jump in value of σ, ε and v after arrival of the elastic wave front. These two jump conditions result from equating impulse to change of momentum for the traversing of an element of the bar by the shock wave and from a consequence of the continuity of displacement across the shock, respectively. These conditions allow the computation of σ, ε and v along the elastic wave front so that points in the interior of the mesh in the x–t plane can be determined.

The initial conditions are

$$\sigma(x, 0) = v(x, 0) = \varepsilon(x, 0) = 0 \qquad x > 0$$

and the boundary condition is

$$\sigma(0, t) = f(t) \qquad t \geq 0$$

which is a function which approximates the stress vs. time record at the first quartz crystal location at the impact end of a long bar in a wave propagation test.

Numerical solution

The computer program written for the solution of the nonlinear algebraic equations which resulted from the finite differencing of equation (9), included a variable mesh size scheme [10, 18]. At $t = 0$, and for short times thereafter, the derivatives of all three variables are quite large. To minimize discretization error the program started with a $\Delta t = 10^{-10}$ sec or $\Delta x = 2 \times 10^{-5}$ in.; later in time these sizes were changed to $\Delta t = 5 \times 10^{-7}$ sec or $\Delta x = 1 \times 10^{-1}$ in. when the time derivatives were greatly reduced in magnitude.

Determination of the "g" function

In order to employ the data plotted in Fig. 4 to predict the propagation of a plastic stress wave in a long bar, the data must be expressed in a functional form. Several investigators have proposed particular functionals in describing the rate sensitivity of certain materials. Some of these are listed below in which the rate sensitivity is expressed by the "g" function [Note: $\dot{\varepsilon}_p = \dot{\varepsilon} = g(\sigma, \varepsilon)$ for $\dot{\sigma} = 0$ from equation (6)] in which $\bar{\sigma}$ is the

$g(\sigma, \varepsilon)$	Domain	Investigator
$K(\sigma - \sigma_y)$	$\sigma > \sigma_y$	Sokolovsky [19]
$K(\sigma - \bar{\sigma})$	$\sigma > \bar{\sigma}$	Malvern [12]
$K(\sigma/\bar{\sigma})^n$	$\sigma > \bar{\sigma}$	Chiddister [2]
$K\left[\frac{\sigma - \bar{\sigma}}{\bar{\sigma}}\right]^n$	$\sigma > \bar{\sigma}$	Chalupnik [4]

value of stress at strain ε in a quasi-static test, σ_y is the static yield stress and both K and n are material parameters which depend only on environmental conditions such as ambient temperature or pressure. In describing the data, one attempts to determine values for the parameters, K and n, which permit the functional form to provide the best fit to the data. Each of the functional forms was tried in an attempt to describe the data shown in Fig. 4. The form which provided a good fit to the data is the fourth one above proposed by Chalupnik. The functional is of such a form that if $\log_{10}[(\sigma - \bar{\sigma})/\bar{\sigma}]$ is plotted vs. $\log_{10} \dot{\varepsilon}_p$ the data points lie on a straight line, the slope of which yields n and the intercept of which yields K. The data from Fig. 4 were plotted on such a log plot (Fig. 8). As Fig. 8 shows, the data points do not lie along a straight line; however, they do lie inside a linear band. Thus,

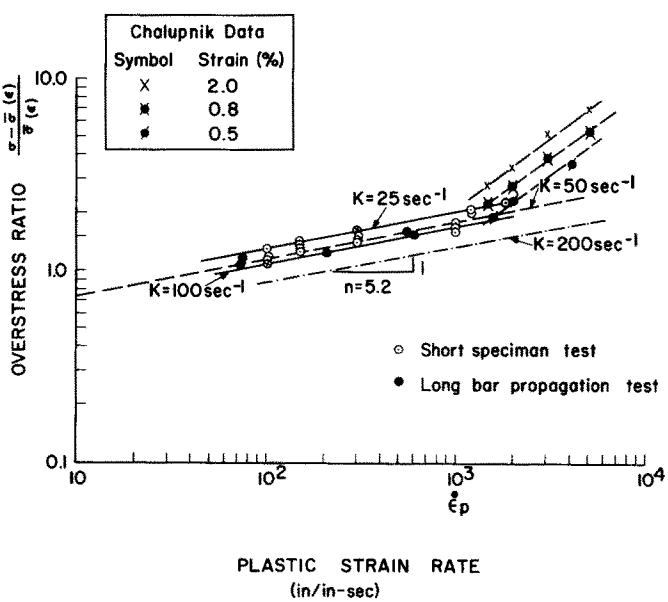

FIG. 8. Log–log plot of overstress ratio vs. plastic strain rate for Armco iron at room temperature.

this functional form could be used as a first approximation to the constitutive equation for the material. If the dashed line inside the linear band is arbitrarily selected as the line along which the data points are assumed to lie, the values for K and n can be calculated. These values are $K = 50\,\text{sec}^{-1}$ and $n = 5{\cdot}2$. The values for K for the upper and lower lines forming the linear band are $K = 25\,\text{sec}^{-1}$ (upper) and $K = 100\,\text{sec}^{-1}$ (lower).

Once the constants K and n are obtained, the constitutive equation can be numerically integrated to yield stress–strain curves for constant strain rates. Thus for

$$\dot{\varepsilon} = \lambda = \text{constant}$$

then

$$\varepsilon = \lambda t$$

and the constitutive equation

$$\frac{\partial \varepsilon}{\partial t} = \frac{1}{E}\frac{\partial \sigma}{\partial t} + K\left[\frac{\sigma - \bar{\sigma}(\varepsilon)}{\bar{\sigma}(\varepsilon)}\right]^n$$

can be written as

$$\frac{\mathrm{d}\sigma}{\mathrm{d}t} = E\left(\lambda - K\left[\frac{\sigma - \bar{\sigma}(\lambda t)}{\bar{\sigma}(\lambda t)}\right]^n\right) \tag{9}$$

which can be numerically integrated for values of stress σ at each strain ε for the given strain rate λ. These curves were calculated for several values of K. Curves for two of these values $K = 50\,\text{sec}^{-1}$ and $25\,\text{sec}^{-1}$ are superposed on the experimental data in Fig. 4. Neither of the two sets of curves matches the data exactly, the curves for $K = 25\,\text{sec}^{-1}$ fitting the data better at the higher strain rates and $K = 50\,\text{sec}^{-1}$ fitting the data better at the lower strain rates.

COMPARISON OF THEORETICAL PREDICTIONS WITH EXPERIMENTAL OBSERVATIONS

The "g" function obtained from the short specimen tests was inserted into the program along with numerical values for Young's modulus and the density of iron. The boundary condition for $\sigma(0, t)$ for $t \geq 0$ used in the program was taken from the stress record at $x = 0$ from a long bar test. In Fig. 10 the dashed curve, which is an approximation to the experimental stress record at $x = 0$, is used as the boundary condition. The programming was greatly simplified by assuming the stress boundary condition to be a step function followed by a polynomial function of time.

The numerical solutions for strain and stress for three values of K are shown superposed on their experimental counterparts in Figs. 9 and 10 respectively. The general overall agreement between experiment and theory is quite good for $K = 50\,\text{sec}^{-1}$ and $n = 5{\cdot}2$ up to 0·8 per cent strain. All four strain curves at the second location reveal the large strain at the elastic front, more than twice the static yield strain, and the concave upward curvature immediately behind the wave front. Possibly, better agreement could be obtained from a better functional representation of $\sigma(0, t)$; however, the constitutive law itself, is only a first approximation to the data, the values of K and n being computed from the dashed line (Fig. 5), for experimental data only up to 0·6 per cent strain. Better agreement

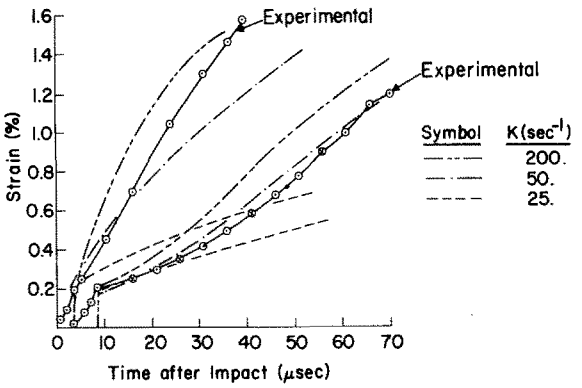

FIG. 9. Typical long bar test data for strain vs. time at two locations. Superposed on test data are three numerical solutions for three different values of K.

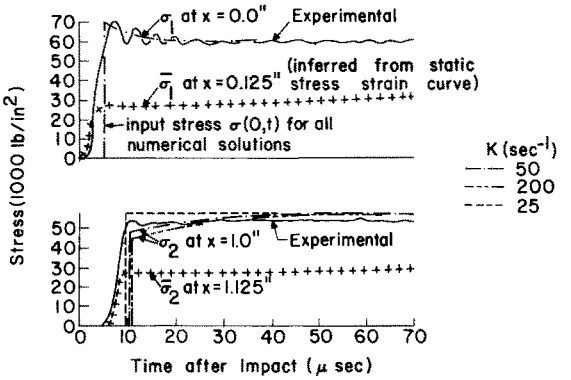

FIG. 10. Typical long bar test data for stress vs. time at two locations. Superposed on test data are three numerical solutions for three different values of K.

might be also attained for $\varepsilon > 0{\cdot}7$ per cent by allowing K and n to be functions of ε and extending the range of strain in the short specimen tests beyond 0·6 per cent strain.

COMPARISON OF TEST DATA AND CONSTITUTIVE EQUATION WITH OTHER INVESTIGATORS

Delay in yield

For reasons already explained, the data reported here were gathered in low stress–rate regions. Since the region of the delay in yield phenomenon, ordinarily observed in rapid testing of iron and steel, occurs in a high stress rate region near the quasi-static yield strain, a region in which lateral inertia effects are expected to be large, this author did not feel justified in drawing any strong conclusions with regard to the stress observed during the delay in yielding phenomenon. However, this author does believe that the increase in stress observed during the delay in yield phenomenon is partly due to material properties and partly due to lateral inertia effects. This author did not expect the yield delay effect to be large compared with the strain rate effect because of the large grain size of the test

specimens. Campbell and Marsh [20] found the time delay for yielding for mild steel to be inversely proportional to the grain size cubed. However, Elam [21] and Chalupnik [22] did not find the stress caused by the yield delay effect to be significant as compared to the strain rate effect. Apparently the delay in yield effect is much greater for mild steel than for pure annealed iron. This author found the stress in the delay in yield region to be no more than 10 per cent above the total stress level in the following region.

Outside of the region of yield delay ($\varepsilon > 0{\cdot}2$ per cent) the test results reported here agree qualitatively with those reported by Elam. A quantitative comparison is not possible since all of Elam's data are for relatively low loading rates. Furthermore, the strain rate is not known. Taylor and Rice [23] found that a good fit to their test data taken from plate impact tests on Armco iron to be a pressure-dilation–dilation rate constitutive equation similar to that proposed by Sokolovsky [19]. This equation is a first order approximation of equation (9), the type of constitutive equation found to provide a good fit to the data reported in this paper. Their tests were conducted at extremely high rates of straining well beyond the strain rates reported here. Chalupnik [22] found his test data for longitudinal impact tests on pure iron to be approximated by the same functional form as did this author. However, his tests were conducted at high strain ($\varepsilon > 0{\cdot}5$ per cent) and strain rate ($\dot{\varepsilon} > 10^3$) levels, levels somewhat higher than those levels reported here. He also chose different $\bar{\sigma}(\varepsilon)$ at $\dot{\varepsilon} = 1$ in./in.-sec rather than at $\simeq 10^{-5}$ in./in.-sec as did this author. Some of Chalupnik's data points are replotted on Fig. 8 for $\log_{10}[(\sigma - \bar{\sigma}(\varepsilon))/\bar{\sigma}(\varepsilon)]$ vs. $\log_{10}\dot{\varepsilon}$ using his values for σ, ε and $\dot{\varepsilon}$ and the value for $\bar{\sigma}(\varepsilon)$ at $\dot{\varepsilon} \simeq 10^{-5}$ in./in.-sec that this author used. One can see in Fig. 8 that Chalupnik's data falls within a linear band which has a greater slope than the linear band for the data reported in this work which lies to the left of $\dot{\varepsilon} = 2{\cdot}10^3$ in./in.-sec. The two linear bands of data agree only at the intersection of the bands between $\dot{\varepsilon} = 10^3$ in./in.-sec and $\dot{\varepsilon} = 2{\cdot}10^3$ in./in.-sec where data points from both bands have a common strain rate. However, the slopes and intercepts of the two linear bands are vastly different. This either indicates the material behavior deviates greatly at higher strain rates from the constitutive functional shown to fit the data at the lower strain rates or that lateral inertia effects are significant beyond $\dot{\varepsilon} \simeq 2{\cdot}10^3$ in./in.-sec. Hunter and Davies [14] derived a relationship for the additional axial stress Σ caused by the lateral inertia effect to be $\Sigma = \frac{1}{2}\rho a^2 \nu^2 \ddot{\varepsilon}$ in which ρ is mass density, a is the bar radius, ν is Poisson's ratio in the plastic range and $\ddot{\varepsilon}$ is the time rate of change of strain rate. If one selects $\nu = \frac{1}{2}$, then for a $\frac{1}{2}$ in. diameter iron bar Σ is of the order of $10^{-5}\,\ddot{\varepsilon}$ psi. From Chalupnik's strain–time data, average time rates of change of strain rate from 10^8 sec^{-2} to 10^9 sec^{-2} are common for strain rates exceeding 10^3 sec^{-1}. Thus, Σ is of the order of 10^3–10^4 psi, enough to shift the linear band up in the high strain rate region, where high lateral inertia effects are expected. Whether or not the apparent change in rate effect at the strain rate of $2{\cdot}10^3$ sec^{-1} is a material property or a lateral inertia effect, the fact remains that separation of strain rate effects from lateral inertia effects in high strain rate regions is very nearly impossible for this type of test. For the higher rates of straining, plate impact tests (one-dimensional strain tests) should provide more reliable data.

CONCLUSIONS

It can be concluded from the results of the tests and numerical solutions described in this paper that pure iron is a highly strain rate sensitive material and that the strain rate sensitivity within the ranges of strain, strain rate and stress rate to which this study was

limited can be approximated by the function

$$\frac{\partial \varepsilon}{\partial t} = \frac{1}{E}\frac{\partial \sigma}{\partial t} + K\left(\frac{\sigma - \bar{\sigma}}{\bar{\sigma}}\right)^n$$

for $E = 28 \times 10^6$ psi, $n = 5{\cdot}2$ and $25\ \text{sec}^{-1} < K < 100\ \text{sec}^{-1}$, the value of $K = 50\ \text{sec}^{-1}$ being the value which best fits the data. Furthermore, the function (for $K = 50\ \text{sec}^{-1}$) can be employed along with the equations of motion and continuity to predict, with reasonable agreement, the stresses and strains occurring in a long bar of pure iron during a wave propagation experiment.

Acknowledgments—The author wishes to express his appreciation to Professor E. A. Ripperger of the University of Texas for his guidance during the experimental undertakings. The author is grateful for the partial financial support of this work at different times by the Army Research Office Contract DA-31-124-ARO-D-229, by the National Science Foundation Grant No. GK-3493, and by the Office of Naval Research Contract No. N00014-68-A-0515.

REFERENCES

[1] A. Nadai and M. J. Manjoine, High speed tension tests at elevated temperatures (Parts II and III). *J. appl. Mech.* **8**, A77–A91 (1941).
[2] J. L. Chiddister and L. E. Malvern, Compression impact testing of aluminum at elevated temperatures. *Exp. Mech.* **3**, 81–90 (1963).
[3] C. H. Karnes and E. A. Ripperger, Strain rate effects in cold worked high-purity aluminum. *J. Mech. Phys. Solids* **14**, 75–88 (1966).
[4] J. D. Chalupnik and E. A. Ripperger, Dynamic deformation of metals under high hydrostatic pressure. *Exp. Mech.* **6**, 547–554 (1966).
[5] J. F. Bell, Single temperature dependent stress–strain law for the dynamic plastic deformation of annealed face-centered cubic metals. *J. appl. Phys.* **34**, 134–141 (1963).
[6] J. J. Gilman, Progress in the microdynamical theory of plasticity. *Proc. Fifth U.S. nat. Congr. appl. Mech.* 385–405 (1966).
[7] H. Watson and E. A. Ripperger, Dynamic stress–strain characteristics of metals at elevated temperatures. *Exp. Mech.* **9**, 289–295 (1969).
[8] F. E. Hauser, J. A. Simmons and J. E. Dorn, *Response of Metals to High Velocity Deformation*, p. 93. Interscience (1960).
[9] G. P. Devault, The effect of lateral inertia on the propagation of plastic strain in a cylindrical rod. *J. Mech. Phys. Solids* **13**, 55–68 (1965).
[10] E. A. Ripperger and Hal Watson, Jr., The relationship between the constitutive equations and one-dimensional wave propagation. *Mechanical Behavior of Materials under Dynamic Loads*, edited by U. S. Lindholm. Springer (1968).
[11] H. Watson, Jr., The effects of strain-rate and temperature on the stress–strain characteristics of copper and iron. Unpublished Ph.D. Thesis, The University of Texas (1967).
[12] L. E. Malvern, Plastic wave propagation in a bar of material exhibiting a strain rate effect. *Q. appl. Math.* **8**, 405–411 (1951).
[13] J. H. Shea, Propagation of plastic strain pulses in cylindrical lead bars. *J. appl. Phys.* **39**, 4004–4011 (1968).
[14] S. C. Hunter and E. D. H. Davies, The dynamic compression testing of solids by the methods of the split Hopkinson pressure bar—I. The theoretical mechanics of the experiment. Armament Research and Development Establishment Report No. MX 8/60, Fort Halstead, Kent, England (1960).
[15] G. J. Cooper and J. W. Craggs, The propagation of plane waves in plastic solids, *J. Aust. math. Soc.* **5**, 349–394 (1965).
[16] B. D. Tapley and H. J. Plass, Jr., The propagation of plastic waves in a semi-infinite cylinder of a strain-rate dependent material. *Proc. Fifth midwest. Conf. Solid Mech.* 256–268. (1961).
[17] C. H. Karnes, B. J. Thorne and W. Hermann, Two dimensional elastic plastic behavior of a rod subjected to axial impact. *Proc. Fifth U.S. nat. Congr. appl. Mech.* 568 (1966).
[18] E. A. Ripperger and Hal Watson, Jr., Strain-rate effects and plastic wave propagation in aluminum rods. *Proc. Fifth U.S. nat. Congr. appl. Mech.* 585 (1966).
[19] V. V. Sokolovsky, The propagation of elastic–visco-plastic waves in bars. *Prik. Mat. i Mek.* **12**, 261–280 (1948).

[20] J. D. CAMPBELL and K. J. MARSH, The effect of strain rate on the post field flow of mild steel. *J. Mech. Phys. Solids* **11**, 49 (1963).
[21] C. F. ELAM, The influence of rate of deformation on the tensile test with special reference to the yield point in iron and steel, *Proc. R. Soc.* **165**, 568–591 (1938).
[22] J. D. CHALUPNIK, The effect of a hydrostatic state of stress on the propagation of plastic waves in metals. Doctoral dissertation, University of Texas (1964).
[23] J. W. TAYLOR and M. H. RICE, Elastic–plastic properties of iron. *J. appl. Phys.* **34**, 364–371 (1963).

(*Received* 5 *June* 1969; *revised* 23 *October* 1969)

Абстракт—Исспытаются короткие цилиндрические образцы из железа Армко, при комнатной температуре, под влиянием сжимаемой осевой нагрузки, при деформациях достигающих 0,6% и скоростях деформации достигающих 10^3 сек$^{-1}$. Во время нагрузки, измеряются осевое напряжение с помощью пъезоэлектрического диска, вставленного между образцом и нагруженным стержнем. Измеряютсоверхность деформации с помощью эпоксидовых присоедниненых пленочных датчиков. Определяется скорость деформации путем дифференцирования записи данных для деформации от времени. Даются графики данных: напряжение—деформация—скорость деформации. Оказываютя возможным аппроксимировать графики с помощью частного конститутивного функционала. Используется конститутивное уравнение вместе с уравнениями движения и непрерывностм для получения численного решения задачи, по распространению одномерной пластической волны в чуствительньм к скорости стержне, вследствие начального осевого напряжения $\sigma(0, t)$. Получается надлежащая сходимость численных решений так для напряжений как и деформаций, вследствие наличия пьезоэлектрических дисков и датчиков напряжений, вдоль двух мест исследования по распространению волны в длинном железном стержне. Затем, можно использовать конститутивную зависимость, которая аппроксимирует данные напряжение-деформация-скорость деформации, возникших при испытании удара коротких образцов, для определения, с умеренно хорошей сходимостью, напряжений и деформаций, измеряемых при исследовании распространения волны в длинном стержне. Эта сходимость указывает свойства течения материала, для широкого круга наблюдаемых деформацмй и скорости деформации.